Characterization of the lithium beam emission spectroscopy at ASDEX Upgrade

M. Willensdorfer[1]‡, G. Birkenmeier[2], R. Fischer[2], F. M. Laggner[1], E. Wolfrum[2], G. Veres[3], F. Aumayr[1], D. Carralero[2], L. Guimarãis[4], B. Kurzan[2] and the ASDEX Upgrade Team

[1] Institute of Applied Physics, Vienna University of Technology, Association EURATOM-ÖAW, A-1040 Vienna, Austria

[2] Max-Planck-Institut für Plasmaphysik, EURATOM Ass., D-85748 Garching, Germany

[3] MTA Wigner FK RMI, Association EURATOM, Pf. 49, H-1525 Budapest, Hungary

[4] Associação EURATOM/IST, Instituto de Plasmas e Fusão Nuclear, Instituto Superior Técnico, Universidade Técnica de Lisboa, Portugal

Abstract.

The lithium beam emission spectroscopy (Li-BES) is a powerful diagnostic to resolve the plasma edge density with high temporal and spatial resolution. The recent upgrades of the Li-BES at ASDEX Upgrade and the resulting gain in photon flux allow the plasma edge density to be determined with an advanced level of accuracy. Furthermore, electron density fluctuations are measured using Li-BES. The Li-BES capabilities and limitations to measure electron density profiles as well as density fluctuations are presented. Li-BES is well suited to characterize electron density turbulence in the scrape off layer (SOL) with decreasing sensitivity towards the plasma core. This is demonstrated by simulations as well as by comparisons with other diagnostics. Li-BES is an appropriate tool to study transport phenomena in the SOL over a wide range of plasma parameters due to its robustness and routine usage.

‡ willensdorfer@iap.tuwien.ac.at

1. Introduction

The particle and energy transport in fusion devices usually exceed the neoclassical prediction. This additional anomalous transport is attributed to the impact of turbulence. To characterize the turbulence and its associated transport, diagnostics are needed, which simultaneously measure turbulence and kinetic profiles with sufficiently high temporal and spatial resolution. A diagnostic which delivers simultaneously electron density profiles and density fluctuation measurements is the lithium beam emission spectroscopy (Li-BES) diagnostic. The routine measurements of electron density profiles from Li-BES have been demonstrated on various fusion devices, e.g. ASDEX Upgrade [1], JET [2], TEXTOR [3, 4], DIII-D [5], W7-AS [6] and LHD [7]. Its capability to measure density fluctuations has been well demonstrated in Ref. [8, 9]. Moreover, the lithium beam diagnostics are capable of measuring ion temperature profiles [10], impurity ion density profiles [11, 12], edge current profiles [13, 14] and poloidal velocities [15].

The significant improvements of the Li-BES at ASDEX Upgrade during the last two decades, i.e., (i) an accurate atomic database [16], (ii) an accurate modeling of the beam attenuation in the plasma [17, 18], (iii) a new evaluation approach within the Bayesian framework [1] and (iv) an improved design of the experimental setup [6, 19], have made it to an important and reliable tool for delivering electron density profiles. Its implementation into the integrated data analysis (IDA), which combines various diagnostics within the Bayesian framework [20], enables us to contribute to studies of transient phenomena inside and outside the confined region, e.g. edge localized modes (ELMs), etc [21, 22, 23, 24]. To increase the accuracy of the existing system, we designed and installed a new optical observation system as well as a new data acquisition (DAQ) system. The enhancements in photon flux and in temporal resolution allowed us to measure simultaneously electron density fluctuations and accurate electron density profiles.

The goal of this paper is to characterize the Li-BES for electron density profile and fluctuation measurements using the upgraded system at ASDEX Upgrade. Therefore, its capabilities and limitations are demonstrated for various applications based on a sensitivity study and measurements from the new optical observation system. This paper is arranged as follows. Section 2 describes the setup and the upgrades of the Li-BES system. The new capabilities of the new system regarding the electron density profiles are demonstrated in section 3. The sensitivity of the Li-BES system with respect to fluctuation measurements will be discussed in section 4. Results from density fluctuation measurements are shown in section 5. The paper concludes with a summary and outlook in section 6.

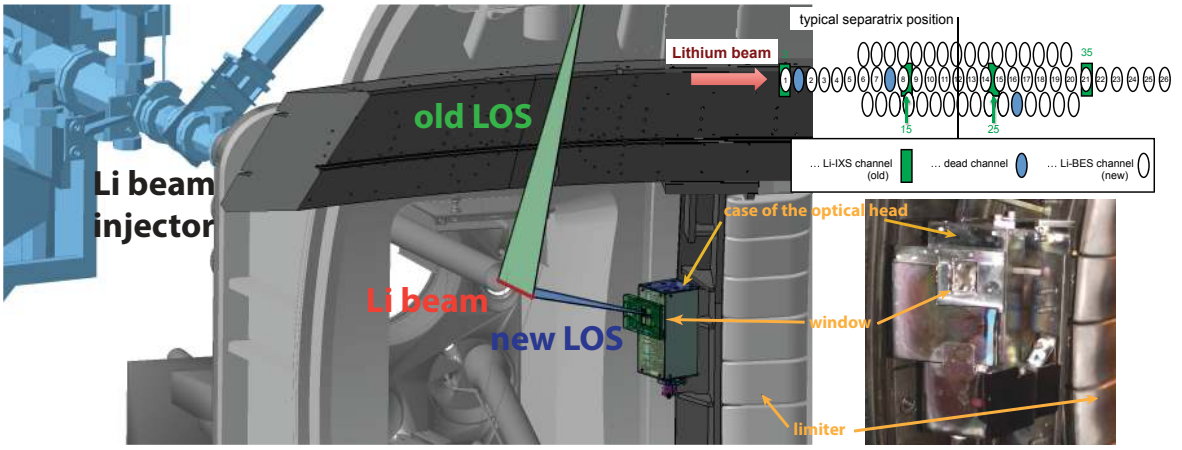

Figure 1. (left) The lines of sight of the old poloidally placed optical head are in green and the lines of sight of the new toroidally placed optical head are in blue. The lithium beam is injected from the low field side and the beam position is indicated by a red line. The lithium beam injector is light blue colored. (right, top) The arrangement of the fiber array is shown. (right, bottom) A photograph of the new optical head is in the right bottom corner.

2. Principle and upgrades of the Li-BES system at ASDEX Upgrade

The Li-BES diagnostics are based on the interaction between the plasma and an injected neutral lithium beam. Due to the collisions between the lithium atoms and the plasma particles, excited atomic states ($Li : 2p, 3s, 3p, 3d, ...$) are populated or the Li atoms are ionized. The most strongly populated state is Li_{2p}, which emits a characteristic photon via radiative de-excitation. This characteristic line intensity is measured along the lithium beam within the plasma. From the spatial distribution of the emission of this line intensity one can deduce electron density profiles using the probabilistic lithium beam data analysis (details in Ref. [1]).

2.1. Lithium beam injector

The lithium beam injector at ASDEX Upgrade produces a neutral lithium beam, which is injected from the low field side (LFS). The current of the generated Li-ion beam ranges between 1.5 and 3 mA with a possible energy range of 35 to 60 keV. Its full width at half maximum (FWHM) is about 12 mm at the observation channels. The maximum power of the lithium beam at ASDEX Upgrade is 180 W and, therefore, not perturbative for the plasma. Newly installed chopping systems allow us to chop the beam by periodically modulating the extraction of the ions and/or by deflecting of the beam aside the optics [23]. Up to 2012, mainly the so-called lithium beam impact excitation spectroscopy (Li-IXS) optics, equipped with interference filters and photomultipliers (PMs), were used to measure electron density profiles (figure 1 in Ref. [23]). The Li-IXS optics were placed above the beam and thus, aligned in the same poloidal plane as the lithium beam. This observation system has 35 channels.

Due to the usage of rectangular fiber bundles, the image is also rectangular with a dimension of 5 mm along the beam and 30 mm perpendicular to the beam. So far, the accuracy and the temporal resolution of electron density profiles from the Li-IXS system were limited by the amount of measured photons as well as by the sampling rate. Therefore, a new optical observation system in addition to a new DAQ system was built to enhance the quality of the electron density profiles and to allow for measuring density fluctuations.

2.2. New optical observation system

In contrast to the old optical system Li-IXS, the new system (in the following called Li-BES optics) was placed toroidally shifted to the lithium beam. Figure 1 shows the arrangement of the injector (light blue), the lithium beam (red) and the lines of sight (LOS) of the old Li-IXS optic (green). The LOS of the new Li-BES optics are shown in blue. From the figure one can already deduce that the LOS of the new system are much shorter. Furthermore, the diameter of the lenses and, hence, the aperture of the new Li-BES optics is larger ($\sim$ 10 cm). Therefore, we expected a significantly higher photon yield. To cover the entire width of the beam without losing in radial resolution (along the lithium beam), the system is anamorphic to be able to image an elliptical volume in a circular fiber core, with different de-magnifications in x- and y-direction. The image of each channel is elliptical with a width of about 6 mm radial to and 12 mm perpendicular to the lithium beam. The right upper corner of figure 1 shows the arrangement and elliptical shape of the different channels. The blue colored channels mark broken fibers. For comparison, 4 channels from the Li-IXS optics are indicated by green rectangles. To measure electron density profiles and poloidal velocities, the new LOS are arranged into 3 rows. 28 channels are placed in the middle row for electron density profile measurements as well as 16 channels above and below the middle row for poloidal velocity measurements via time delay estimation. This paper focuses on electron density profile and density fluctuation measurements using the middle row. The channels of the middle row were equipped with interference filters (671.5 ± 1.5 nm) corresponding to the red shifted $\mathrm{Li}_{2\mathrm{p}-2\mathrm{s}}$ line and PM systems to ensure a high temporal resolution. To protect the optical system from additional in-vessel contamination, e.g. from boronization, a moving glass window is installed in front of the optics and a piezo drive based shutter system is used to move it.

2.3. X-Y deflection plates and background subtraction

So far, it was only possible to move the beam in the toroidal plane (green LOS in figure 1). This was necessary to either align the beam and/or to chop the beam by deflection for background subtraction. Because of the toroidally arranged new Li-BES optics, we also added a second pair of deflection plates to deflect the beam in the poloidal plane. This allows us to optimize the beam position for both optics. Additionally, the voltage switching system as reported in Ref. [19, 25] was built to allow for high frequency

hopping between the side rows of the new Li-BES system. The two deflection plates were mounted in series to avoid a quadrupole effect, which can defocus the beam.

Since the optical systems view the lithium beam poloidally and toroidally, simple hopping of the beam in one plane does not necessarily chop the lithium signal in both optics. To ensure a proper background subtraction in both optics simultaneously, we mainly used the extraction chopping technique, which modulates the voltage responsible for the ion extraction. Thus, it modulates the beam intensity. For more details see Ref. [19]. Thus, the deflection plates were mainly used to optimize the beam position.

2.4. New DAQ system and photon statistics

To increase the temporal resolution, we installed a new DAQ system (called SIO) [26] with 96 channels and a sampling rate of 200 kHz. Both optical systems are equipped with the new DAQ system, which simplifies the comparison between the two systems. Figures 2(a-d) show time traces of the line emission of one channel from the old (figure 2(a,b) in green) and one from the new optics (figure 2(c,d) in blue) at the same radial position on the lithium beam. The rectangular signal shape originates from the 56 ms *beam on* and the 24 ms *beam off* phase. First, it should be noted that the chopping of the beam appears more distinct in the measurements of the new Li-BES optics. Second, the signal to noise ratio is enhanced by a factor of 10 to 40. Both facts indicate a significant increase in photon flux. This improved photon statistics are also reflected by the scatter in the emission profiles. Figure 2(f) shows the emission profiles of the new system and figure 2(e) of the old system versus the normalized poloidal magnetic flux surface coordinate (ρ_{pol}). The emission profiles of the new system exhibit considerably less scatter than the old system. The calibration procedure described in Ref. [1] allows us to determine the photon counts via Poisson statistics. From this calibration procedure, a gain in photon flux $50 - 100$ times larger compared to the old system is determined. This enhancement originated from the shorter LOS, the larger aperture and since, it is a new system, the photon yield is not reduced from any degradation, e.g. boron layer and neutrons.

3. High accuracy electron density profiles

To evaluate electron density profiles using the new system, we employed the probabilistic lithium beam analysis based on the Bayesian probability theory (BPT) described in Ref. [1]. The significant increase in the photon statistics appreciably improves the quality of the electron density profiles. Figure 3 compares the emission profiles (figure 3(a,b)) and the corresponding electron density profiles (figure 3(c,d)) during low confinement mode (L-mode) (left row) and high confinement mode (H-mode) (right row). The data points are binned to 50 μs within a time window of 1 ms. Again, the emission profiles from the Li-BES optics show less scatter. This enables us to determine a more accurate electron density profile, although the new system is only equipped with 26 instead of

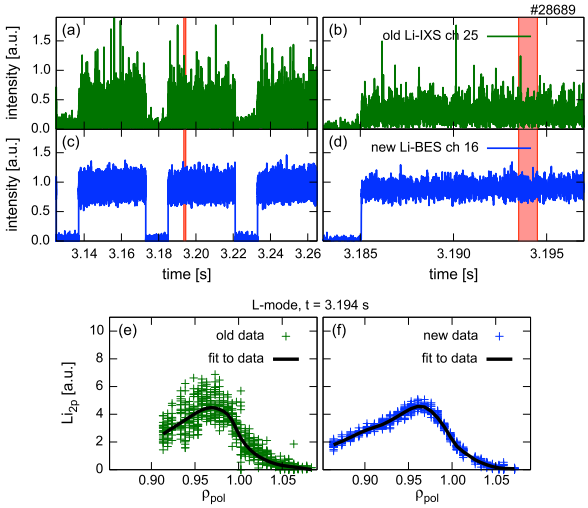

Figure 2. Time traces of two channels at the same radial position from (a,b) the old and (c,d) the new system. The left time traces show data within 150 ms and right within 20 ms. The temporal resolution is 5 μs. The corresponding emission profiles from (e) the old system and (f) the new system. The emission profile points are binned to 50 μs within a time window of 1 ms. The selected time window of 1 ms for the emission profile is indicated by the red shaded area. The new system (blue color) delivers data with a significantly higher signal to noise ratio.

35 channels. Both systems agree very well in the scrape off layer (SOL), but in the confined region, the enhancement of the new system is clearly demonstrated. Due to the higher photon statistics, the pedestal top is better resolved and, furthermore, the uncertainties are smaller. Moreover, the emission profiles of both systems lie on top of each other indicating a reliable spatial calibration (figure 3(a,b)).

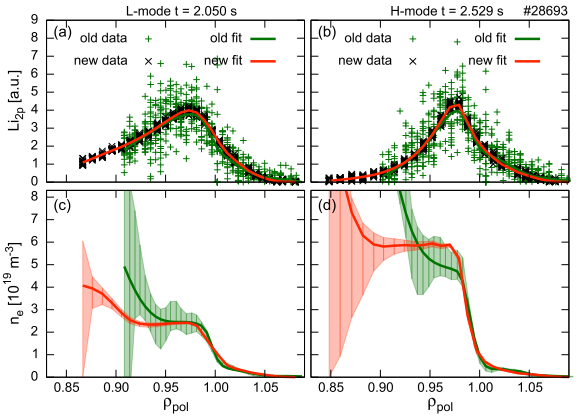

Figure 3. Comparison of the old (green) and new (red) system. (a,b) Emission profiles in L-mode and in H-mode are shown. (c,d) Corresponding density profiles in L-mode and in H-mode. The electron density profiles agree very well in the SOL, but profiles from the new system are more accurate in the confined region.

To compare the density profiles from the Li-BES system with other diagnostics, dedicated experiments were performed in which various electron density diagnostics

at ASDEX Upgrade measured simultaneously. A comparison between the Li-BES, Reflectometry (REF) [27, 28], core and edge Thomson scattering (TS) [29] diagnostics during a radial plasma sweep in ohmic L-mode is shown in figure 4. The electron density profiles agree well within the uncertainties. Only in the pedestal top region the various diagnostics differ slightly.

Due to the considerable improvement of the signal to noise ratio of the Li-BES measurement small deficiencies in the relative calibration can be easily detected. Hence, an additional magnetic shielding of the PM system was necessary. Additionally, the analysis is more sensible on the provided electron temperature profiles, which requires the modeling due to the implementation of temperature dependent rate coefficients. But In principle, the improvements and the gain in photon flux allows electron density profiles to be delivered with a temporal resolution of 5 μs.

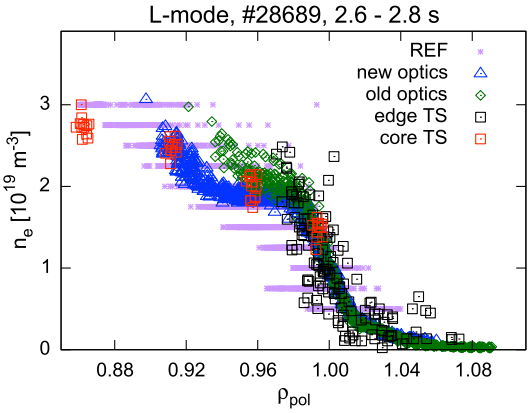

Figure 4. Comparison of the electron density profiles from Li-BES using the new optical system (blue triangles) and the old one (green diamonds), the core and edge Thomson scattering system [29] (rectangles) and the reflectometer system (REF) [30] (purple stars) during a radial plasma sweep in L-mode. The diagnostics agree very well within their uncertainties.

4. Li-BES Sensitivity

Before analyzing fluctuation measurements using Li-BES, a sensitivity study was performed to investigate the reliability of fluctuation measurements from Li-BES data at ASDEX Upgrade. Similar studies were done at the W7-AS stellerator [31]. A modified tanh-function [32] was used to provide an analytical expression of an L-mode density profile. A Gaussian with a FWHM of 2 cm was added to the tanh-profile to simulate a density perturbation. The resulting emission profile was calculated with and without this perturbation. The amplitude δn_e and the position of the density perturbation was varied, and for each parameter set the emission profile was calculated. Figure 5 shows a density profile (red color) with a perturbation $\delta n_e/n_e$ of 100% in the SOL (a) and at the pedestal top (b). For the x-axis, the beam position along the beam path into

the plasma is used, where 0 corresponds to the position, at which the beam enters the vessel chamber. The corresponding emission profiles are shown in black. The density perturbation in the SOL is clearly reflected by a perturbation in the emission profile, which has about the same amplitude as the original n_e perturbation (dashed in figure 5). However, the positions between the two perturbations are shifted. The additional density perturbation leads to an additional population of the Li_{2p} state, which then undergoes radiative de-excitation. Because of the finite lifetime of the Li_{2p} state of about 27.11 ns, half of the Li_{2p} populated atoms de-excites within 1.99 cm assuming a beam energy of 40 keV. As a result, the Gaussian density perturbation is seen smeared out and shifted in the calculated emission profile.

For density perturbations at the pedestal top, the signatures in the emission profile changes. Figure 5(b) shows a 100% density perturbation at the pedestal top. Instead of a pronounced perturbation in the emission profile, a sustained decrease in the emission profile is seen. Before the maximum of the emission profile, the population via electron excitation from the Li_{2s} ground state to the Li_{2p} state is the dominant process and electron density structures are well reflected by the emission profile. Towards the maximum of the emission profile, the de-population of the Li_{2p} state becomes more important and at the maximum it is equal to its population of it [17]. After the maximum the Li_{2p} de-population plays the dominant role and the density structures are reflected by an additional decrease of the emission profile. Because of the decreasing number of Li atoms in the Li_{2s} ground state, the population of the Li_{2p} state from the Li_{2s} ground state becomes towards the core negligible. Thus, the density perturbation is mainly seen by a de-population of the Li_{2p} state to higher states or ionization. This explains the decrease in the emission profile in the subsequent channels and the non-local response of the emission profile (grey in figure 5) on the density perturbation.

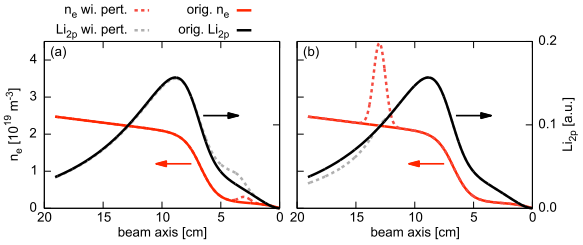

Figure 5. Light emission profiles (black) and electron density profiles (red) are shown with perturbation (dashed) and without perturbation (solid). 100% density perturbation (a) in the SOL and (b) at the pedestal top.

This study was extended to a parameter scan, in which the position and the amplitude of the n_e perturbation were scanned. For each amplitude and position value, the maximum amplitude of the emission profile perturbation was calculated. Figure 6 shows the normalized amplitude of the emission perturbation $\delta Li_{2p}/Li_{2p}$ depending on the density perturbation $\delta n_e/n_e$ for different positions (color scaling). This sensitivity study reveals that perturbations in the SOL are well measurable by the Li-BES. For

example, the relative amplitude of the emission and density perturbations have about the same value in the first centimeters along the beam axis. The points are close to the black solid line, which corresponds to a ratio between $\delta \mathrm{Li}_{2p}/\mathrm{Li}_{2p}$ and $\delta \mathrm{n_e}/\mathrm{n_e}$ of 1. Towards the plasma core, the sensitivity decreases. In the case around the maximum of the emission profile ($\sim$ 8 cm), a density perturbation of 10 % causes a fluctuation of only 1 % in the emission profile. This lowered sensitivity is related to the beam attenuation.Since the density fluctuations in the confined region are typically in the range of $\delta n_e/n_e \sim 10 - 20$ % [33], it is rather unlikely that the Li-BES is capable to resolve such fluctuations. Moreover, the density perturbations after the maximum of the emission profile are measured by a non-local decrease of the emission profile.

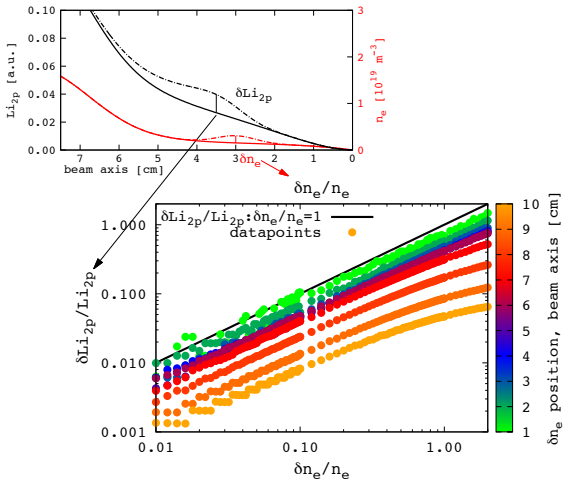

Figure 6. The perturbation study shows the normalized amplitude of the emission perturbation ($\delta \mathrm{Li}_{2p}/\mathrm{Li}_{2p}$) depending on the density perturbation ($\delta n_e/n_e$) at different positions (color scaling). One density perturbation and the corresponding density illustrated in the top figure. The original density is the same as in figure 5 and the maximum of the emission profile is at 8 cm. The black solid line indicates the ratio between $\delta \mathrm{Li}_{2p}/\mathrm{Li}_{2p}$ and $\delta n_e/n_e$ of 1.

From this sensitivity study one can conclude that density perturbations or fluctuations up to the maximum of the emission profile can be well localized and resolved by the new Li-BES optics. Beyond the maximum, Li-BES is relatively insensitive to small perturbations and the mentioned non-locality makes the fluctuation measurements within the pedestal top region challenging. In the confined region, only large perturbations and coherent structures are detectable (see section 5.2). Please note that the position of the maximum of the emission profile depends on the plasma density. For higher plasma densities the beam attenuation is higher and the maximum shifts towards the wall. Thus, low density plasma discharges are more appropriate to study density fluctuations using Li-BES.

One should also keep in mind that this insensitivity in the pedestal top has also an impact on the density reconstruction. Small systematic deviations in the emission profile measurements, e.g. due to inaccurate calibration or non-linearity of PMs, can result in

artificial structures in the reconstructed density profile. High calibration precision of the optics and DAQ system, especially for channels viewing the confined region, is needed to resolve the entire electron density profile accurately.

5. Density fluctuation measurements

The sensitivity study in section 4 shows that the Li-BES is capable of measuring fluctuations in the SOL, but measurements around the pedestal top are challenging. In the following sections, we will demonstrate and discuss these capabilities of the Li-BES system to detect fluctuations using measurements from the ASDEX Upgrade experiment. For the following study, we mainly used the signals from the emission profile to avoid complications due to density profile parameterization and regularization.

5.1. Frequency spectra using Li-BES

One way to characterize density fluctuations is to calculate the frequency spectra of the emission signal. Since the measured line emission does include in addition to density fluctuations, also photon and amplifier noise, one has to employ an analysis method which separates the noise from density fluctuations. Thus, we calculated the averaged cross power spectra (CPS) between two neighboring channels of several 2 ms long sub-intervals using

$$CPS = \frac{1}{N}\left|\sum_{i=0}^{N}\left\{\left(\int_{t_i}^{t_{i+1}} x(t)e^{-i\omega t}dt\right)^{*}\int_{t_i}^{t_{i+1}} y(t')e^{-i\omega t'}dt'\right\}\right| \tag{1}$$

where N corresponds to the total number of averaging time windows, x the time trace of the analyzed channel, y the signal of the neighboring channel and $*$ the complex conjugate. Since the photon and the amplifier noise of two neighboring channels are not correlated, the phases of incoherent contributions cancel out in the averaged time window and only plasma induced fluctuations should contribute to the CPS as long as the plasma fluctuations cover more than one channel. To get a sufficiently high reliability, we averaged the spectra within a period of several 100 ms.

To check the self-consistency of the Li-BES system, we shifted the plasma radially in steps of $5-6$ mm ($\sim$ distance between two channels) during an ohmic L-mode discharge. The plasma remained for several 100 ms on each position, while other plasma parameters, e.g. density, were kept constant. This method allowed us to compare measurements from different channels at the same ρ_{pol} position.

Figure 7(a) shows the emission profile versus ρ_{pol} for different plasma positions. The small changes in the emission profiles arise from changes in the beam intensity and different lengths of the beam path. The green shaded areas in figure 7(a) indicate the 4 radial positions used for the CPS. The CPS during ohmic L-mode for *beam on* (red) and *beam off* (black) phase at a ρ_{pol} of $1.04, 1.02, 1.00$ and 0.98 are shown in figure 7(b),(c),(d) and (e), respectively. Several points are remarkable: (i) The CPS of the *beam on* part has a significantly higher amplitude than during *beam off*, which indicates

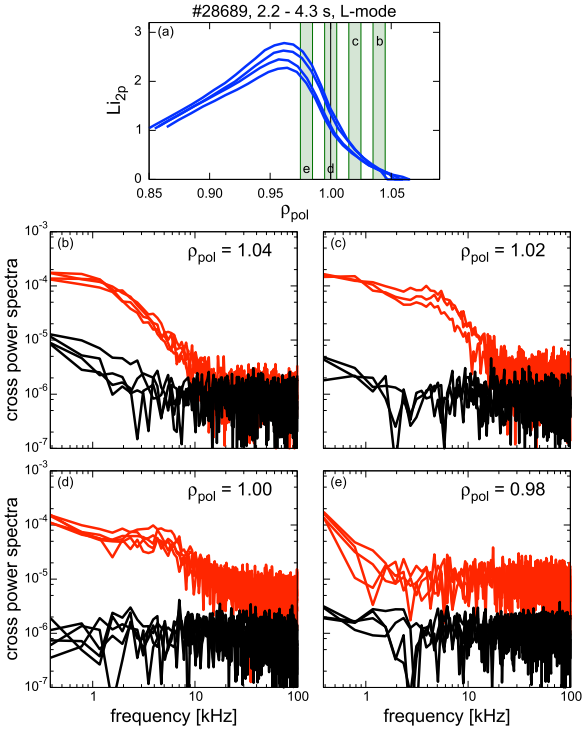

Figure 7. (a) Emission profiles for different radial plasma positions. The green shaded areas indicate the radial range for the analysis. (b)-(e) Cross power spectra for *beam on* (red) and *beam off* (black) at a ρ_{pol} of (b) 1.04, (c) 1.02, (d) 1.00 and (e) 0.98. Each spectrum in one plot is from a different radial position channel due to the radial shifts of the plasma. Each panel shows 4 traces during *beam on* and *beam off* at the same ρ_{pol}.

that we actually measure density fluctuations and not background fluctuations (figure 7(b-e)). (ii) All spectra show that the Li-BES delivers self-consistent data: e.g. in figure 7(b), the 4 different red lines correspond to spectra of 4 different channels, which were measured at the same ρ_{pol}, but during different discharge phases. Different channels at the same ρ_{pol} position measure the same CPS during the *beam on* and *off* phase, which proves the self-consistency of this diagnostic. (iii) All channels in the SOL observe low frequency events $f < 10$ kHz and a flat CPS at higher frequencies $f > 30$ kHz. (iv) In the confined region (figure 7(e)), the low frequency feature mentioned in point (iii) disappears and only events with a frequency lower than 1 kHz in almost all channels remain.

In the following, we will discuss the low frequency events $f < 1$ kHz in the confined region. These events occur in every channel in the confined region. Thus, it is presumed that these events could be an artifact from the SOL due to the beam attenuation. To validate this, a digital low-pass filter of 2 kHz was applied and the normalized cross-correlations between two reference channels as well as all other channels were calculated. Figure 8 shows the cross-correlation using a reference channel viewing the SOL at $\rho_{pol} \sim 1.03$ (figure 8(a) and (b)). The channels in the confined region ($\rho_{pol} < 0.96$)

clearly anti-correlate with the ones in the SOL for low frequency events ($f < 2$ kHz), which confirms our suspicion that the channels in the confined region are influenced by the SOL fluctuations via beam attenuation: A large density event in the SOL, i.e. blob, excites the Li-neutrals to higher states or ionization leading to a missing fraction of Li_{2p} states in the confined region. This is very pronounced in L-mode due to the high fluctuation level in the SOL. Furthermore, the cross-correlation of the channels within $\rho_{pol} = 0.90 - 0.98$ remain at about the same level indicating that almost all channels are equally influenced.

The spatio-temporal cross-correlation function in figure 8(b) also enables us to deduce the radial propagation velocity. This low frequency SOL events in figure 8(b), indicates an outwards directed radial propagation visible in the tilt with respect to the x-axis (indicated by a white arrow), which is not seen in the confined region. Hence, in combination with poloidally displaced channels and the time delay estimation, it is possible to determine radial and poloidal propagation velocities.

In principle, fluctuations in the reconstructed density profile should not show the anti-correlation between inner and outer channels. But due to the reduced density information beyond the emission maximum this is difficult to be shown.

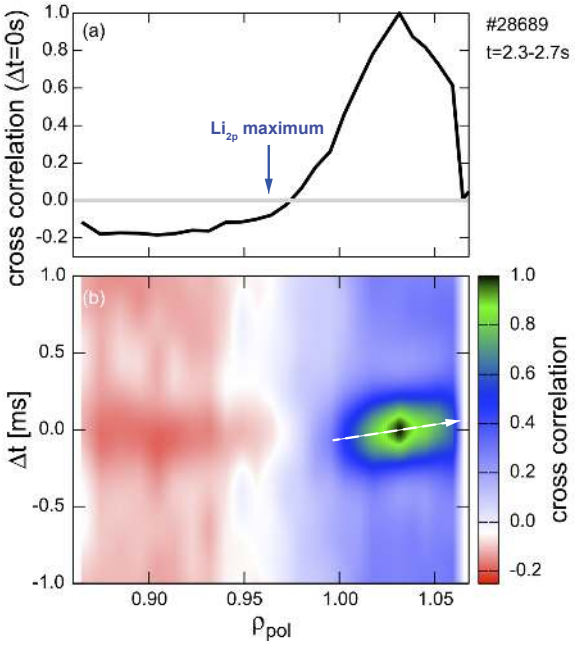

Figure 8. (a) The cross correlation between channels where the reference channel is in the SOL ($\rho_{pol} \sim 1.03$). The position of the Li_{2p} maximum is indicated by the blue arrow. (b) Spatio-temporal correlation function using a reference channel in the SOL. The white arrow indicates the direction of radial propagation. The low-frequency fluctuations in the SOL clearly impact the measurements in the confined region indicated by the anti-correlation.

5.2. Li-BES spectra in comparison to other diagnostics

To validate Li-BES results, they are compared to results from probe and REF data. In figure 9, a strong activity for $f < 10$ kHz in the CPS is shown, which decays towards higher frequencies (red). The results from the PM systems are supported by avalanche photo diodes (APDs), a different DAQ system and a sampling rate of 500 kHz (not shown). For further analyses, a comparison with Langmuir probe measurements at the mid plane was drawn. Figure 9 shows the CPS from Li-BES (red: *beam on* phase, black: *beam off* phase) and the auto power spectrum (APS) of the probe ion saturation current to compare both measurements during L-mode (figure 9(a)) and H-mode (figure 9(b)) at the same radial position. The spectra from the probe measurements were scaled to the maximum frequency of the Li-BES spectra. The spectra of the two different diagnostics show an excellent agreement in different plasma scenarios. During L-mode (figure 9(a)), both diagnostics observe a kink at ~ 4 kHz. The amplitude is decreasing with higher frequencies. This indicates that blobs in the SOL mainly occur at lower frequencies. The CPS of the Li-BES at higher frequencies $f > 30$ kHz remains at the same level, whereas the spectrum of the ion saturation data continuously decreases. The image size of the optics is 6 mm $\times$ 12 mm, whereas the probe has a diameter of < 2 mm [34]. Therefore, structures with a perpendicular wavenumber $k_\perp$ larger than the corresponding wavenumber of the observation volume cannot be resolved, because of $\omega = v_\perp k_\perp$ depending on $k_\perp$ and the perpendicular velocity $v_\perp$. Thus, density fluctuations with frequencies $f > 30$ kHz are not resolved. They show a white noise characteristics (no f dependency). The low-frequency events in the SOL are well reflected in the Li-BES signal. Furthermore, the probe and the Li-BES spectra (figure 9(b)) also show an excellent agreement during the type-III ELMy H-mode.

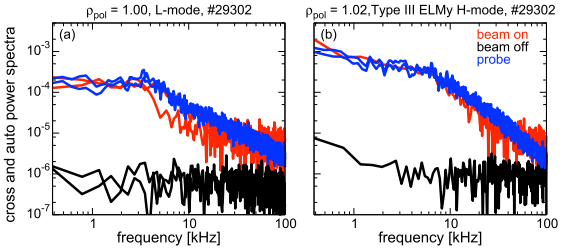

Figure 9. (a) The cross power spectra from Li-BES and auto power spectrum from probe measurements at the separatrix during L-mode. (b) Same as (a) but in the SOL during type-III ELMy H-mode. Both diagnostics show a similar frequency dependency.

The sensitivity study in section 4 shows a decreasing sensitivity of the Li-BES towards the plasma core. Although the sensitivity suffers from the decreasing beam intensity, it is still possible to resolve mode activities, if the mode amplitude is sufficiently large and $k_\perp$ is small enough to be detected within our observation volume. Examples for such activities, which were detected by Li-BES, are neoclassical tearing modes (NTMs) and quasi-coherent (QC) modes. Figure 10 shows a QC-mode [35] at 50 kHz measured by Li-BES and reflectometry [36] during the ELM-free H-mode. The measurements

agree very well. This QC mode could also be measured by neighboring Li-BES channels at $\rho_{pol} \sim 0.94 - 0.97$.

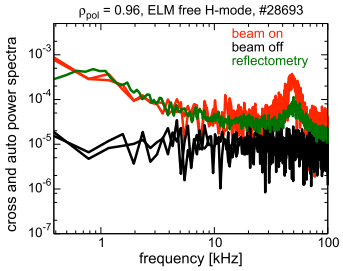

Figure 10. The cross power spectra from Li-BES and auto power spectrum from reflectometry measurements in the confined region are shown during an ELM-free H-mode. The reflectometry signal was scaled to the same level. Both diagnostics observe the same quasi-coherent mode at 50 kHz.

6. Summary and Outlook

We have shown that the Li-BES spectroscopy is capable of determining edge electron density profiles and electron density fluctuations simultaneously. The new optical observation system and DAQ system enables us to reconstruct electron density profiles with high accuracy. The significantly higher flux of detected photons increases the spatial and temporal accuracy of the density profiles. The measurements of the new system are in-line with the measurements from the old system and from other diagnostics.

The recent upgrades of the Li-BES also allows us to measure electron density fluctuations. On the one hand, the Li-BES system is ideal to study the intermittent transport in the SOL over a wide range of plasma parameter due to its routine usage. This is underlined by a sensitivity study and demonstrated by an inter-diagnostic comparison. But on the other hand, the detection of density fluctuations in the pedestal top region is rather challenging, even with a very good photon statistics. The reasons for this are: (i) Li-BES is insensitive to small density perturbations in this region, (ii) density perturbations appear non-local in the emission profile and (iii) the measurements in the pedestal region are also influenced by SOL perturbations via beam attenuation. Although the Li-BES is not suitable to detect density fluctuations at the pedestal top, it is still possible to resolve large coherent and quasi-coherent structures.

It is planned to investigate the capabilities of Li-BES to measure poloidal velocity measurements using the side rows of the optical system. Furthermore, Li-BES will be used to study the intermittent transport and a blob size scaling study is currently ongoing [37]. The high temporal resolution and the low uncertainties of the electron density profiles will allow us to study transient transport phenomena in more detail.

7. Acknowledgement

The authors thank J. Schweinzer and S. Zoletnik for fruitful discussions. M. Willensdorfer is a fellow of the Friedrich Schiedel Foundation for Energy Technology. This work, supported by the European Commission under the Contract of Association between EURATOM and ÖAW, was carried out within the framework of the European Fusion Development Agreement (EFDA). The views and opinions expressed herein do not necessarily reflect those of the European Commission.

[1] R. Fischer et al. *Plasma Physics and Controlled Fusion*, 50(8):085009, 2008.
[2] M. Brix et al. *Review of Scientific Instruments*, 83(10):10D533, 2012.
[3] I. Pusztai et al. *Review of Scientific Instruments*, 80(8):083502–083508, 2009.
[4] E. Wolfrum et al. *Review of Scientific Instruments*, 64(8):2285–2292, 1993.
[5] H. Stoschus et al. *Review of Scientific Instruments*, 83(10):10D508, 2012.
[6] S. Fiedler et al. *Journal of Nuclear Materials*, 266-269:1279–1284, 1999.
[7] T. Morisaki et al. *Review of Scientific Instruments*, 74(3):1865–1868, 2003.
[8] D. Thomas et al. *Review of Scientific Instruments*, 61(10):3040–3042, 1990.
[9] S. Zoletnik et al. *Physics of Plasma*, 6:11, 1999.
[10] M. Reich et al. *Plasma Physics and Controlled Fusion*, 46(5):797, 2004.
[11] R. P. Schorn et al. *Applied Physics B: Lasers and Optics*, 52:71–78, 1991.
[12] E. Wolfrum et al. *Review of Scientific Instruments*, 77(3):033507, 2006.
[13] D. Thomas et al. *Physical Review Letters*, 93(6):065003, 2004.
[14] K. Kamiya et al. *Review of Scientific Instruments*, 81(3):033502–033502–8, 2010.
[15] S. Zoletnik et al. *Plasma Physics and Controlled Fusion*, 54(6):065007, 2012.
[16] J. Schweinzer et al. *Atomic Data and Nuclear Data Tables*, 72(2):239–273, 1999.
[17] J. Schweinzer et al. *Plasma Physics and Controlled Fusion*, 34(7):1173–1183, 1992.
[18] R. Brandenburg et al. *Plasma Physics and Controlled Fusion*, 41:471–484, 1999.
[19] M. Willensdorfer et al. *Review of Scientific Instruments*, 83(2):023501, 2012.
[20] R. Fischer et al. *Fusion science and technology*, 58(675–682), 2010.
[21] A. Burckhart et al. *Plasma Physics and Controlled Fusion*, 52(10):105010, 2010.
[22] E. Wolfrum et al. *Plasma Physics and Controlled Fusion*, 53(8):085026, 2011.
[23] M. Willensdorfer et al. *Nuclear Fusion*, 52(11):114026, 2012.
[24] M. Willensdorfer et al. *Nuclear Fusion*, 53(9):093020, 2013.
[25] S. Zoletnik et al. *Review of Scientific Instruments*, 76(7):073504–12, 2005.
[26] K. Behler et al. *Fusion Eng. Des.*, 2010.
[27] L. Cupido et al. *Review of Scientific Instruments*, 75(10):3865–3867, 2004.
[28] L. Cupido et al. *Review of Scientific Instruments*, 77(10):10E915, 2006.
[29] B. Kurzan et al. *Review of Scientific Instruments*, 82(10):103501, 2011.
[30] A. Silva et al. *Review of Scientific Instruments*, 70(1):1072–1075, 1999.
[31] S. Zoletnik et al. *Plasma Physics and Controlled Fusion*, 40(7):1399, 1998.
[32] R. Groebner et al. *Physics of Plasma*, 9(5):2134–2140, 2002.
[33] B. Nold et al. *Plasma Physics and Controlled Fusion*, 52(6):065005, 2010.
[34] H.-W. Müller et al. *Nuclear Fusion*, 51(7):073023, 2011.
[35] S. da Graça et al. *40th Conf.EPS Plasma Phys. (Espoo, 1–5 July 2013)*, 2013.
[36] S. da Graça et al. *Plasma Physics and Controlled Fusion*, 49(11):1849, 2007.
[37] G. Birkenmeier et al. *40th Conf.EPS Plasma Phys. (Espoo, 1–5 July 2013)*, 2012.